



Article

Seismic Assessment of Six Typologies of Existing RC Bridges

Pietro Crespi ¹, Marco Zucca ^{1,*}, Nicola Longarini ¹ and Nicola Giordano ²

¹ Department of Architecture, Built Environment and Construction Engineering, Politecnico di Milano, 20133 Milan, Italy; pietro.crespi@polimi.it (P.C.); nicola.longarini@polimi.it (N.L.)

² Department of Civil Engineering, University of Bristol, Bristol BS8 1TR, UK; nicola.giordano@bristol.ac.uk

* Correspondence: marco.zucca@polimi.it

Received: 25 May 2020; Accepted: 25 June 2020; Published: 26 June 2020



Abstract: Over the last few decades, the attention on the safety of existing reinforced concrete (RC) structures has significantly increased. RC bridges, in particular, are highly relevant for strategic importance. In the Italian context, several of these bridges were built around 1960, when engineering practice commonly ignored or underestimated the presence of seismic actions. Therefore, it is fundamental to quantify as accurately as possible their seismic safety level with state-of-the-art analysis techniques. In this paper, an efficient procedure based on the multi-modal pushover analysis approach is proposed for the risk evaluation of several bridges of the Italian highway network. This procedure, tailored for portfolio level assessment, takes into account the non-linear behavior and the complex dynamic response this type of structure with limited computational effort. Three fundamental aspects are defined for the structural modelling of bridges, i.e., materials' constitutive law, finite element type and nonlinear hinge models. Flexural and shear nonlinearities of piers are included to account for ductile and brittle damage potential. The standardized procedure guarantees consistent comparisons among different bridges of the same network in the form of risk indexes.

Keywords: highway bridges; seismic vulnerability; multi-modal pushover analysis

1. Introduction

During last years, several collapse phenomena have affected existing reinforced concrete (RC) bridges that led to considerable interest on the evaluation of the residual capacity of these structures under static and dynamic loads [1,2]. For this reason, several researches have presented different types of approaches in order to evaluate the safety level of the existing bridges or of other types of strategic infrastructures [3–10]. In the Italian Highway Network, the majority of these bridges were built in the 1960s and 1970s. Nowadays they require several maintenance operations in order to ensure standard safety levels. Moreover, according to new design codes, particular attention is given to the seismic capacity evaluation assessment of these structures. For instance, the Italian Civil Protection requires highway managing operators to collect relevant data of each asset in their portfolios and to conduct nonlinear seismic assessments for emergency planning and investment prioritization purposes [11].

Several issues remain arises when evaluating the seismic response of existing reinforced concrete (RC) bridges with nonlinear techniques [3]. On one hand, standard nonlinear pushover analysis, which is nowadays widely used in structural engineering firms, e.g., [12], fails to address the complex dynamic response of bridges that are not characterized by a predominant vibration mode. On the other hand, nonlinear time history analyses involve several challenges for professional engineers such as ground motion selection, modeling of strength/stiffness degradation, high computational cost, etc. [13]. An alternative solution presented in the literature is the Modal Pushover Analysis

(MPA) that was initially developed by Chopra and Goel [14,15] to assess the seismic response of unsymmetrical-plan buildings. The MPA consists of an extension of the Response Spectrum Analysis (RSA), particularly effective for irregular structures that do not exhibit a principal mode shape with high participating mass. The methodology was further extended to the case of bridges thanks to the work of Kappos et al. [16,17].

In this paper, an efficient procedure is proposed in order to evaluate the seismic vulnerability of bridges taking into consideration the above-mentioned aspects. This procedure is based on the implementation of Finite Element Models (FEM) where the non-linear behavior of the piers is represented with concentrated plastic hinges that consistently reduce the computational effort allowing the execution of MPA analyses. The result of the assessment is expressed in terms of Risk Index, i.e., the ratio between the maximum Peak Ground Acceleration (PGA) that the bridge can withstand (capacity) and the PGA of the site asset at stake for the given location (demand). The procedure is applied to six representative case studies of a bridge portfolio characterized by cantilever and frame type piers. The results are discussed highlighting the critical aspects of each typology with respect to their seismic behavior.

2. Multi-Modal Pushover Approach

Pushover analysis is commonly used for the evaluation of the non-linear behavior of an existing structure or infrastructure subjected to an incremental horizontal load. Three base concepts regulate the application of the pushover analysis [18]: (a) the capacity curve, (b) the demand spectrum and (c) the performance point.

The capacity curve defines the nonlinear response of a structure subjected to a predefined lateral load distribution. The curve usually consists in a top displacement versus base shear diagram. The shape of the lateral load profile is usually proportional to a mode shape:

$$s_n^* = M\phi_n, \tag{1}$$

where: M is the mass matrix of the structure, ϕ_n is the n-th eigenvector, s_n^* is the loading vector applied to the structure during the analysis. The obtained curve can be converted in the spectral displacement (S_d) versus spectral acceleration (S_e) plane through these fundamental relations:

$$S_e = \frac{V_{bn}}{M_n^*}, \tag{2}$$

$$S_d = \frac{u_{rn}}{\Gamma_n\phi_{rn}}, \tag{3}$$

where: V_{bn} is the base shear for the n-th vibration mode, u_{rn} is the top displacement value of the control point for the n-th vibration mode, M_n^* is the modal mass of the n-th mode, Γ_n is the modal participation factor and ϕ_{rn} is the control point component of the n-th eigenvector.

The seismic demand curve can be represented in the Acceleration Displacement Response Spectrum (ADRS) format, obtained from the horizontal acceleration response spectrum using the formula below:

$$S_d = \frac{1}{4\pi^2} S_e T^2 \tag{4}$$

The performance point is obtained by intersecting the capacity curve with the demand curve and represents how the structure would behave under the specific seismic action (Figure 1a).

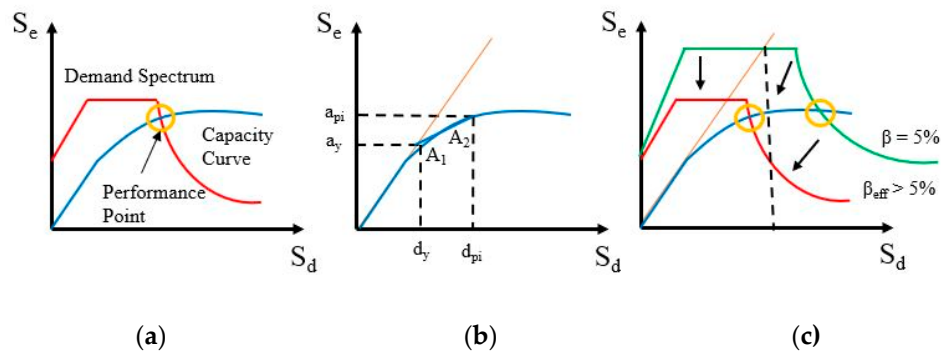


Figure 1. (a) Performance point calculation; (b) Capacity curve idealization; (c) Scaled demand spectrum [9].

Several techniques have been proposed in order to evaluate the performance point. An extended state-of-the-art review is reported by Causevic and Mitrovic [19]. Through a bilinearization of the capacity curve (Figure 1b), a demand reduction coefficient is obtained. This can be evaluated in terms of ductility factor or equivalent damping and takes into account the energy dissipation of the post-elastic phase. The intersection between the reduced demand spectrum and the capacity curve identifies the performance point. In this work, the Capacity Spectrum Method (CSM) technique is adopted [18,20,21] where these fundamental steps are executed:

1. Definition of the seismic demand in the ADRS form;
2. Selection of the first iteration point a_{pi} , d_{pi} on the capacity;
3. Bilinearization of the capacity curve with K_I as elastic stiffness followed by a hardening branch. The hardening branch is defined by applying the equal energy rule between the capacity curve and its bilinear idealization (Figure 1b);
4. Scaling of the ADRS according to the effective damping coefficient. This takes into consideration both the hysteretic damping (referred to the cyclic plastic deformations) and the inherent damping (equal to 5% in the case of concrete structures), Figure 1c;
5. Evaluation of the performance point by intersecting the capacity curve and the scaled demand spectrum through an iterative process.

The selection of the horizontal load profile for the pushover analysis is not univocal and can decisively influence the results. As discussed in the Introduction, there has been consistent research on the topic, e.g., [13]. In this work, mode-shape load profiles are adopted as for Chopra and Goel [14]. Operationally, N capacity curves are determined, one for each significant vibration mode. For each capacity curve, the performance point is evaluated with reference to the same seismic demand spectrum. Lastly, relevant internal-forces/displacements at the performance configuration are extracted and combined with the classical modal combination rules (e.g., CQC).

3. Structural Modelling

A fundamental step in assessing the seismic vulnerability of existing structures is the determination of the actual materials' characteristics through the execution of laboratory/in-situ tests. It is worth mentioning that, within the same structure, the variability of mechanical properties can be high. Therefore, the Italian Building Code [11,22] requires the use of an appropriate confidence factor that is related to the level of knowledge obtained through the survey campaign. Consequently, materials' strength is reduced for structural verifications. In absence of specific laboratory investigations, concrete and steel mechanical properties are taken from technical-scientific studies [23,24].

The materials' constitutive laws should take into account the mechanical phenomena that occur at both element and cross section levels. The concrete behavior is significantly influenced by the confining effect of transverse reinforcement. In this work, the concrete model developed by Kent and Park [25] was chosen, considering only the compressive behavior. The Kent and Park concrete model takes into

account the confining effect of stirrups through the confinement parameter K . The coefficient Z defines the post-peak (softening) response of the material (Figure 2a). For the steel reinforcements, the Park Strain Hardening [26] constitutive law was adopted (Figure 2b).

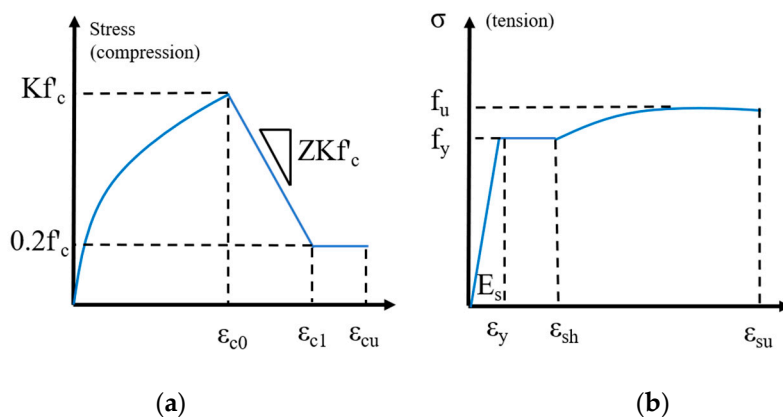


Figure 2. (a) Kent Park constitutive law; (b) Park Strain Hardening constitutive law.

In this work, the FEM models of the reinforced concrete bridges were developed using the software MIDAS Civil [27]. A simplified approach has been adopted where (i) the deck, the piers and the pier cups are schematized with beam elements (ii) the bearings are modeled using general links with stiffness values calculated as in EN 1337-3:2005 [28]. The connection between beam elements and general links is guaranteed thanks to rigid links. The abutments are represented as restrains located at deck-abutments interface bearings base. Lastly, the piers are assumed fixed into rigid foundations. Stiffness reduction due to cracking is taken into account when assessing the natural frequencies of RC structures. This can be done with a specific reduction coefficient of the cross-section elastic stiffness obtained from the moment-curvature ($M-\chi$) diagram, as for EN 1998-2:2005 [29]. Structural and non-structural masses are considered for eigenvalue analysis while traffic loads are neglected [11].

For the nonlinear response of elements two types of mechanisms that characterize piers have been considered: (i) the flexural-ductile mechanism and (ii) the shear-brittle mechanism. The ductile mechanism refers to the rotational capacity of the plastic hinges while the brittle mechanism depends on the shear strength. These two collapse mechanisms interact and affect simultaneously different structural elements. As a result, it is quite complex to obtain a reliable estimate of the nonlinear dynamic response. In this work, the bridges' capacity has been assessed by investigating these failure mechanisms separately.

The ductile response is modeled with concentrated plastic hinges. Figure 3 shows the example related to the piers characterized by a cantilever behavior.

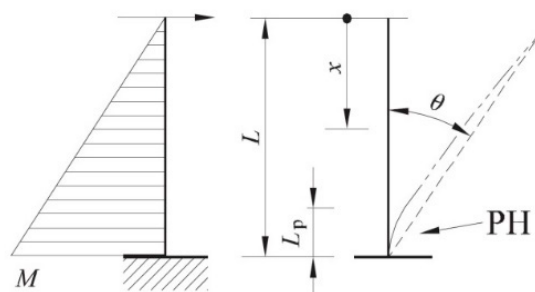


Figure 3. Plastic hinge (PH) of a pier characterized by a cantilever behavior.

These plastic hinges are defined from the moment-curvature ($M-\chi$) diagram of the cross-section. The yield point defines the stiffness of the cracked section. The ultimate curvature determines the

ultimate capacity of the member. The curvature ductility μ_ϑ is the ratio between the ultimate and yield curvatures:

$$\mu_\vartheta = \frac{\chi_u}{\chi_y} \tag{5}$$

The data extracted from the $M-\chi$ curve are incorporated in the moment-rotation diagram by integrating the curvatures over the plastic hinge length (L_{pl}). For constant distribution of the bending moment over L_{pl} , the yield and ultimate rotations are:

$$\vartheta_y = L_{pl} \cdot \chi_y \tag{6}$$

$$\vartheta_u = L_{pl} \cdot \chi_u \tag{7}$$

The plastic hinge length (L_{pl}) is calculated according to the EC8 [29]:

$$L_{pl} = 0.1L_v + 0.17h + 0.24 \frac{d_{bl} \cdot f_y}{\sqrt{f_c}} \tag{8}$$

where: d_{bl} is the diameter of the longitudinal bars, f_y is the yield stress of the steel rebars and f_c is the concrete compressive strength.

The FEMA 356 [20] reports the definition of nonlinear hinge relationships for pushover analysis. The plastic hinge law (Figure 4a) is represented by a linear elastic portion (AB), followed by a hardening branch (BC). The point C refers to the maximum bending capacity of the element. The corresponding rotation defines the point of sudden decrease of capacity (CD). The residual strength is taken as 20% of the maximum moment (DE). Point E corresponds to the complete failure of the element.

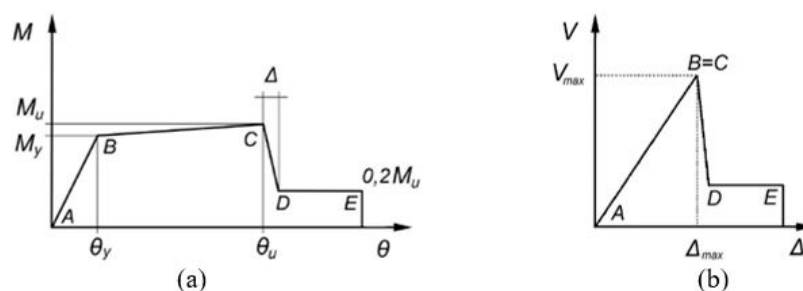


Figure 4. (a) Ductile mechanism; (b) and brittle mechanism.

The verification criterion corresponding to the Life Safety limit state is assumed equal to $\frac{3}{4}$ of the ultimate rotation ϑ_u . The brittle collapse mechanism depends on the shear capacity of the piers. It is worth mentioning that RC bridges were generally designed to resist small lateral loads. Thus, their horizontal bearing capacity (e.g., seismic resistance) is quite low.

In the present work, the shear strength of the piers is assumed according to EC8 [30], where the cyclic shear resistance V_R in the plastic hinge region accounts for the contribution of three factors: (i) the axial load, (ii) the concrete strength and (iii) the transversal reinforcement. An elastic-brittle force-displacement constitutive law is considered in this work [20]. The verification criterion for the Life Safety limit state is assumed equal to the achievement of V_R .

The Italian Building Code [11] requires quantification of the seismic response of the bridge at a given location in terms of risk index. The risk index is the ratio between capacity (C) of the bridge and the seismic demand (D) expressed in Peak Ground Acceleration, PGA (or return period). The PGA_D is directly taken from the seismic hazard map for the given location. The estimation of the PGA_C requires an iterative process. The N pushover curves are intersected with an increasing spectrum until the safety limit on at least one structural member is exceeded. According to the “second level vulnerability assessment form” by the Italian Civil Protection, risk indices are defined as follow [31]:

- Risk index in acceleration (RI_{PGA}): is the ratio between capacity (PGA_C) and demand (PGA_D) in terms of peak ground acceleration;
- Risk index in return period (RI_{TR}): is the ratio between capacity (T_{RC}) and demand (T_{RD}) in terms of return period of the earthquake, raised to 0.41 [11,31].

Values close to one or larger than one characterizes cases where the risk level is acceptable. On the contrary, values close to zero characterizes high-risk cases.

4. Case Studies

The procedure, described in Section 3, has been applied to six different bridges, representative of the Italian Highway Network. In all the models, the longitudinal axis of the bridge is represented by the X axis, while the transversal direction is oriented with Y axis of the coordinate system.

The first bridge (Figure 5) is characterized by the presence of two adjacent and independent carriageways, consisting in a sequence of seventeen simply supported 36 m spans (except for the central span which is 60 m long). The planimetric and altimetric layout is rectilinear. The overall width of the roadway is about 11 m and each span of the bridge is realized by a precast concrete slab of six prestressed U girders. The bridge deck consists in a 20 cm thick concrete slab. Each span of the bridge is supported by 2×6 elastomeric bearings placed at the ends of each longitudinal beam.

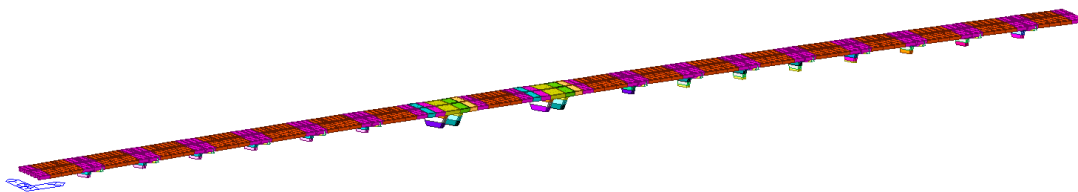


Figure 5. Bridge 1.

Each pier is structurally independent from the adjacent one and it has a rectangular tapered section where the base dimension is equal to 7×2 m while the top dimension is 8×2 m. At the top of every RC pier, there is a hammerhead cap where the elastomeric bearings are located. The piers are made of C25/30 concrete with $74\varnothing22$ longitudinal AQ50 steel rebars confined by $\varnothing10/30$ cm stirrups.

The second viaduct (Figure 6) is also made by two adjacent and independent carriageways. It is constituted by a sequence of five simply supported 22 m length spans, realizing a rectilinear planimetric and altimetric layout.

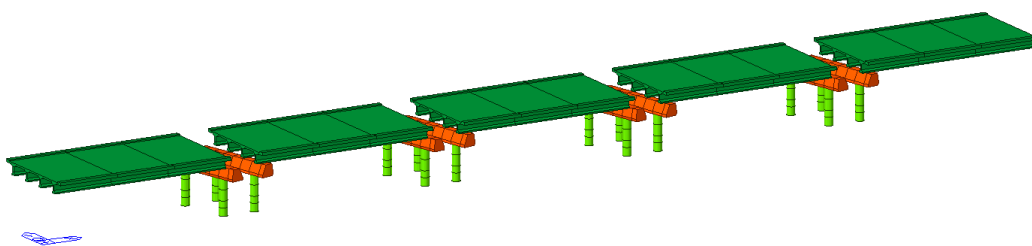


Figure 6. Bridge 2.

The overall width of the roadway is 9.85 m and each span is realized with a precast concrete girder of four I longitudinal beams and four transverse beams. The viaduct deck consists in a 25 cm thick concrete slab. Each span of the bridge is supported by 2×4 elastomeric bearings. In this case, the piers are composed by two independent frames. Each frame has two cylindrical columns (diameter equal to 1 m). The two columns are connected at the top by a trapezoidal beam where the elastomeric bearings are located. The piers' characteristics are: C25/30 concrete, $16\varnothing20$ longitudinal AQ50 steel rebars, $\varnothing8/20$ cm spiral stirrups.

The third case study (Figure 7), is a long span bridge characterized by a total length equal to 77 m. The overall width of the roadway is about 10 m and the long span is realized by a spirall prestressed precast concrete slab while the deck consists in a 20 cm thick concrete slab. The long span is supported by 20 elastomeric bearings divided between the two piers and the abutments.

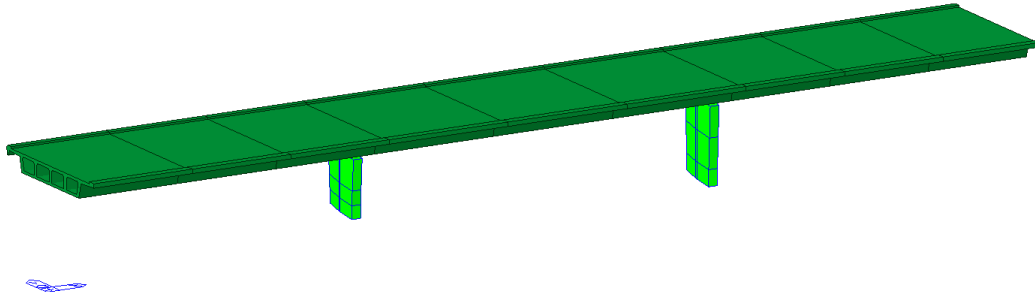


Figure 7. Bridge 3.

Each pier is characterized by a rectangular tapered section which presents a base dimension equal to 5×0.9 m and a top dimension equal to 5.6×0.9 m. The elastomeric bearings are placed in correspondence to the top of the pier. The two piers are made of C20/25 concrete with 38Ø18 longitudinal AQ50 steel rebars confined by Ø10 stirrups having a spacing of 25 cm.

The fourth bridge (Figure 8), is characterized by the presence of two adjacent and independent carriageways. It consists in a sequence of eighteen simply supported 29 m length spans. The layout presents a slight curvature. The overall width of the roadway is about 12 m and each span of the bridge is realized by a precast concrete lattice girder formed by four longitudinal beams (three characterized by an I section and one by a U section) and five transverse beams while the deck consists in a 22 cm thick concrete slab. Each span of the viaduct is supported by 2×4 elastomeric bearings placed at the end of each longitudinal beam.

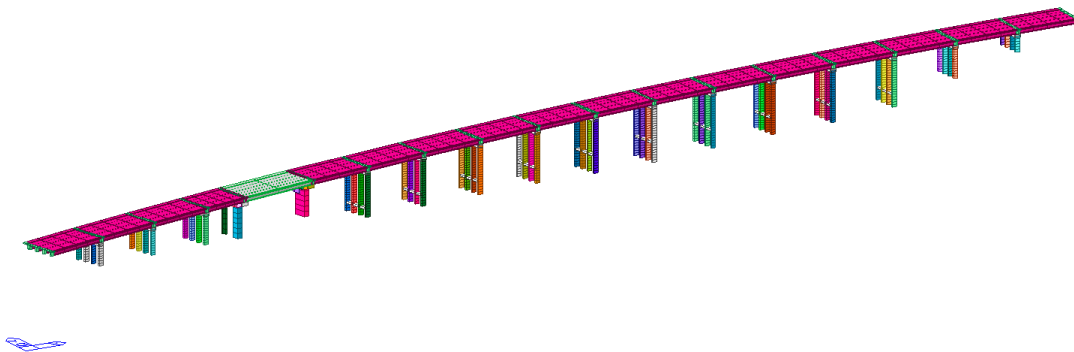


Figure 8. Bridge 4.

The piers are characterized by a frame system consisting of four columns with a rectangular section 0.8×2 m. The fourth pier presents two independent columns characterized by a triangular section and by a rectangular section 3×2.4 m. The fifth pier is composed by a rectangular 6×2.4 m column. The piers are made of C32/40 concrete with 22Ø20 longitudinal FeB44K steel rebars confined by Ø12/20 cm stirrups.

The fifth case study is a long span bridge with a total length equal to 65 m (Figure 9). The overall width of the roadway is 11.25 m and the long span is realized by a precast concrete lattice girder with five longitudinal I beams, seven transverse beams and a 20 cm thick concrete deck. The long span is supported by twenty elastomeric bearings divided between the two frame piers and the abutments.

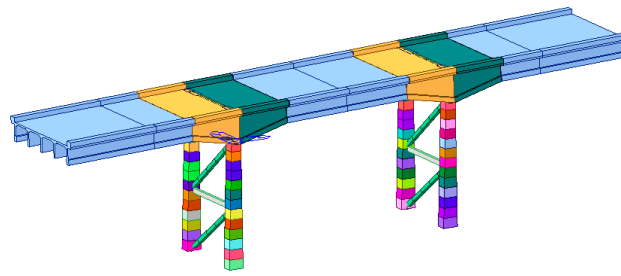


Figure 9. Bridge 5.

Each pier is composed by a reticular concrete frame where the columns are characterized by a rectangular tapered section that varies from 1.06×1.61 m at the base to 1.06×1.36 m. Concrete material is C40/50 with $30\text{Ø}20$ longitudinal FeB44K steel rebars confined by $\text{Ø}12/30$ cm stirrups.

Lastly, the sixth case study consists in a multi span bridge characterized by two simply supported 39 m spans (Figure 10). The overall width of the roadway is about 12 m and each span is realized by a precast concrete lattice girder formed by four longitudinal I beams, four transverse beams and a 20 cm thick deck. Each span of the bridge is supported by 2×4 elastomeric bearings placed at the end of each longitudinal beam.

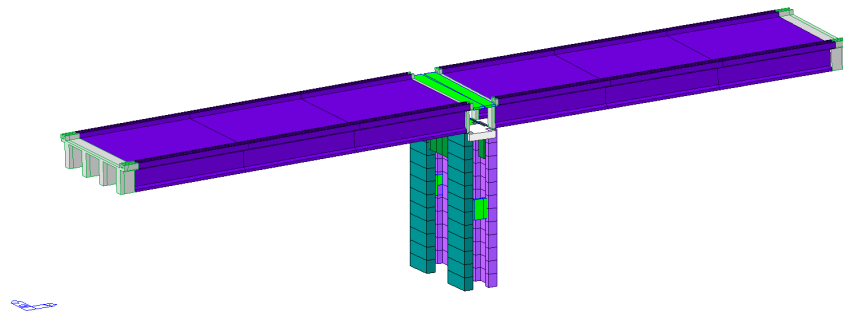


Figure 10. Bridge 6.

The pier is characterized by a spatial frame where four columns present a C section and are made of C28/35 concrete with $50\text{Ø}16$ longitudinal AQ50 steel rebars and $\text{Ø}8/20$ cm stirrups.

The piers of the analyzed case studies are characterized by quite different structural behaviors. Piers of bridge 1 and 3 present a cantilever boundary configuration. Other bridges' piers are characterized by double-clamped (frame) configuration. Figure 11 shows six representative moment-curvature diagrams, one for each of the analyzed bridges.

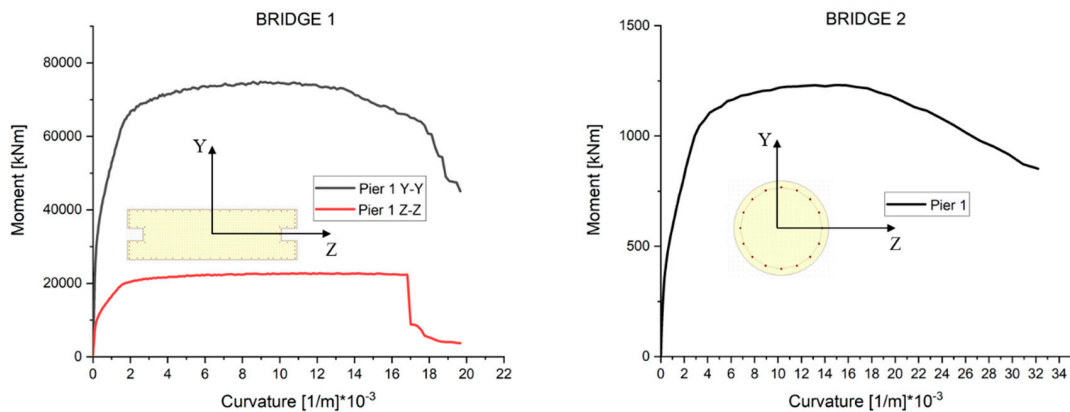


Figure 11. Cont.

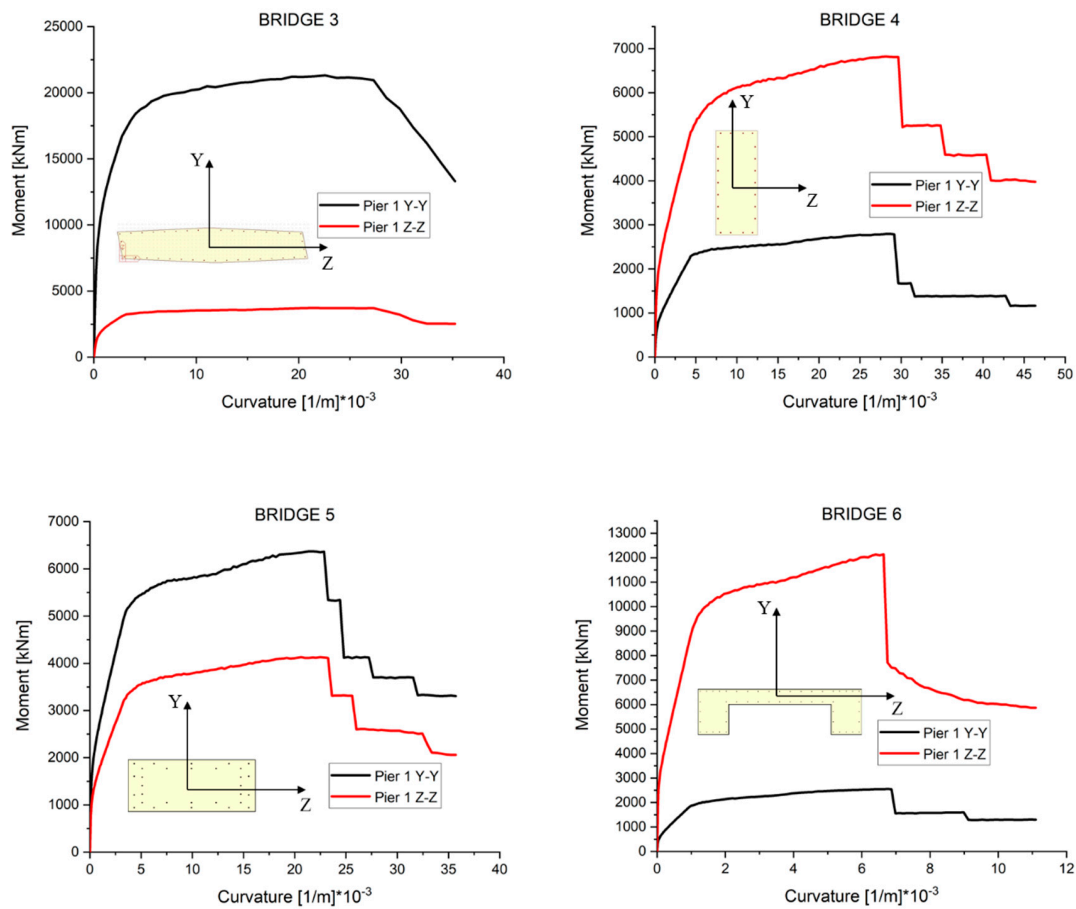


Figure 11. Moment-curvature diagrams of different bridges’ piers.

The idealized moment-rotation relationships of the corresponding plastic hinges are summarized in Table 1.

Table 1. Idealized moment-rotation plastic hinge relationships (Y-Y direction).

Diagram Point (Figure 4a)	Bridge 1 Pier 1		Bridge 2 Pier 1		Bridge 3 Pier 1		Bridge 4 Pier 1		Bridge 5 Pier 1		Bridge 6 Pier 1	
	ϑ [rad]	M [kNm]	ϑ [rad]	M [kNm]	ϑ [rad]	M [kNm]	ϑ [rad]	M [kNm]	ϑ [rad]	M [kNm]	ϑ [rad]	M [kNm]
A	0	0	0	0	0	0	0	0	0	0	0	0
B	0.0005	62310	0.0029	956	0.0007	16611	0.0045	2288	0.0027	4953	0.0014	8796
C	0.0045	73349	0.0186	1223	0.0078	20929	0.0290	2791	0.0174	6339	0.0094	12138
D	0.0045	12462	0.0186	191	0.0078	3322	0.0290	458	0.0174	990	0.0094	1752
E	0.0079	12462	0.0235	191	0.0079	3322	0.0315	450	0.0189	990	0.0098	1752

As previously discussed, the brittle failure is governed by the shear response. The idealized shear-displacement curves of the considered piers are reported in Table 2.

Table 2. Idealized shear-displacement plastic hinge laws (Z direction).

Diagram Point (Figure 4b)	Bridge 1 Pier 1		Bridge 2 Pier 1		Bridge 3 Pier 1		Bridge 4 Pier 1		Bridge 5 Pier 1		Bridge 6 Pier 1	
	Δ [mm]	V [kNm]	Δ [mm]	V [kNm]	Δ [mm]	V [kNm]	Δ [mm]	V [kNm]	Δ [mm]	V [kNm]	Δ [mm]	V [kNm]
A	0	0	0	0	0	0	0	0	0	0	0	0
B	0.3371	2707	0.2430	190	0.1901	738	0.7696	818	0.4853	768	0.4341	424
C	0.3371	2707	0.2430	190	0.1901	738	0.7696	818	0.4853	768	0.4341	424
D	0.3640	541	0.2624	38	0.2053	148	0.8311	164	0.5241	154	0.4688	85
E	1.3485	541	0.9720	38	0.3802	148	1.5392	164	0.9706	154	0.8682	85

Eigenvalue analysis has been performed for each case-study bridge. The most significant vibration modes have been used as modal-horizontal load profiles of the pushover analysis. Natural periods (T_j) and corresponding modal participation mass (m_j) of the vibration mode involving at least 5% of the total mass are listed in Table 3 (longitudinal direction) and Table 4 (transversal direction). These vibration modes are characterized by a prevalent value of participant mass in the longitudinal or transversal direction.

Table 3. Longitudinal vibration modes.

Bridge 1			Bridge 2			Bridge 3			Bridge 4			Bridge 5			Bridge 6		
n°	T_j [s]	m_j [%]	n°	T_j [s]	m_j [%]	n°	T_j [s]	m_j [%]	n°	T_j [s]	m_j [%]	n°	T_j [s]	m_j [%]	n°	T_j [s]	m_j [%]
1	0.932	23.6	2	0.624	73.9	1	0.970	92.4	3	1.293	36.0	1	0.993	84.0	3	1.272	92.3
4	0.881	17.1	6	0.572	10.0	2	0.803	5.8	5	1.085	31.7	6	0.376	10.8	9	0.410	5.6
11	0.791	5.2	25	0.148	9.5	-	-	-	8	0.827	12.4	-	-	-	-	-	-
86	0.205	10.3	-	-	-	-	-	-	-	-	-	-	-	-	-	-	-

Table 4. Transversal vibration modes.

Bridge 1			Bridge 2			Bridge 3			Bridge 4			Bridge 5			Bridge 6		
n°	T_j [s]	m_j [%]	n°	T_j [s]	m_j [%]	n°	T_j [s]	m_j [%]	n°	T_j [s]	m_j [%]	n°	T_j [s]	m_j [%]	n°	T_j [s]	m_j [%]
1	0.932	6.0	1	0.632	70.5	1	0.970	5.8	1	2.051	42.4	3	0.630	6.9	1	1.678	60.5
11	0.791	19.9	5	0.591	10.3	2	0.803	90.5	2	1.621	5.0	5	0.529	76.9	5	0.816	14.4
17	0.776	13.7	23	0.148	9.3	-	-	-	4	1.185	8.1	11	0.255	11.0	6	0.718	10.9
33	0.724	5.6	-	-	-	-	-	-	6	1.046	13.8	-	-	-	15	0.276	5.9
86	0.205	5.7	-	-	-	-	-	-	-	-	-	-	-	-	-	-	-

Figure 12 shows one relevant pushover curve for each of the analyzed bridges where only the nonlinear bending response is considered (ductile mechanism).

Given a specific seismic input (ADRS spectrum), the calculation of the performance point is carried out with the CSM for each relevant capacity curve as in [21]. Subsequently, corresponding internal forces are combined with the CQC technique and compared to the limit state’s maximum capacity.

If the verification is satisfied, the PGA of the selected spectra is lower than PGA_C . Therefore, the procedure has to be repeated with an increased spectrum until PGA_C is detected. This iterative process leads to the calculation of the risk indexes in terms of PGA or return period T_R (RI_{PGA} or RI_{TR} , respectively), i.e., the maximum bearable PGA (or T_R) over the corresponding site design values. Table 5 reports the results of the six bridges for the ductile mechanism.

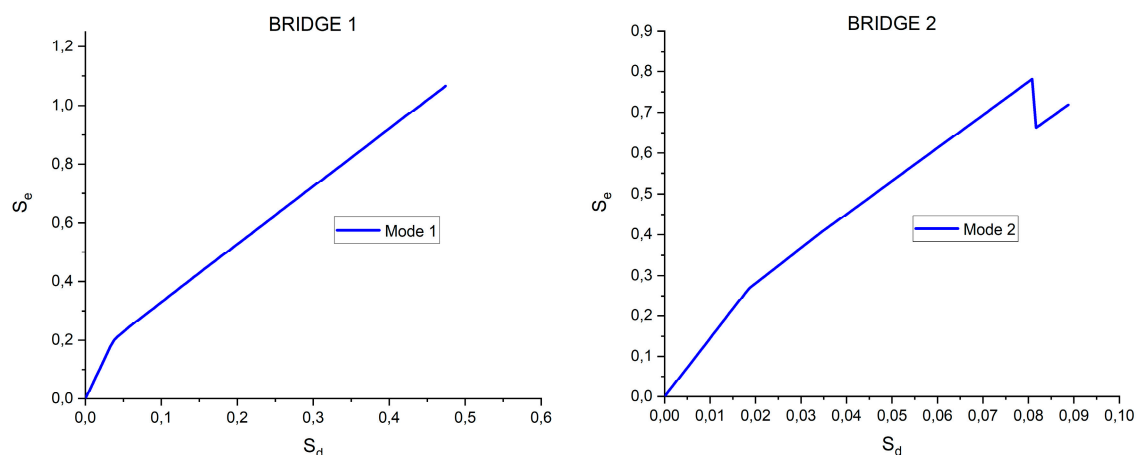


Figure 12. Cont.

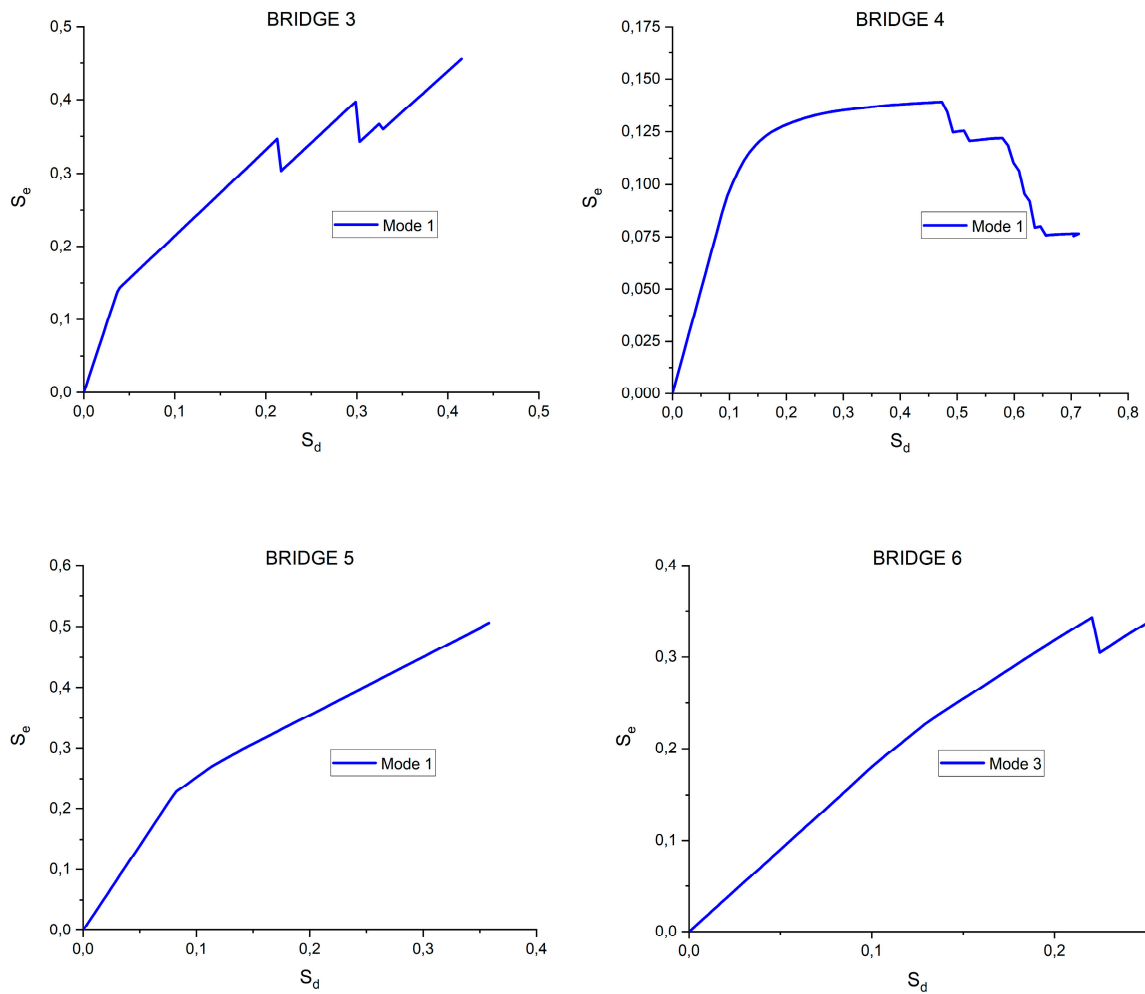


Figure 12. Capacity curves for ductile mechanism (S_e [1/g]– S_d [m]).

Table 5. Risk indexes for ductile mechanism.

	Bridge 1		Bridge 2		Bridge 3		Bridge 4		Bridge 5		Bridge 6	
	Long.	Tran.	Long.	Tran.	Long.	Tran.	Long.	Tran.	Long.	Tran.	Long.	Tran.
PGA_C [g]	0.266	0.266	0.326	0.278	0.509	0.509	0.187	0.201	0.449	0.495	0.232	0.585
T_R [years]	6188	6188	9965	6226	47,968	47,968	480,730	678,299	470,783	655,387	37,983	680,065
RI_{PGA} [-]	1.785	1.785	2.188	1.866	3.416	3.416	3.696	3.973	6.210	6.844	3.256	8.195
RI_{TR} [-]	2.157	2.157	2.622	2.162	4.995	4.995	12.849	14.797	12.740	14.590	4.539	14.813

Analogously, pushover analyses of relevant vibration modes are performed for the brittle mechanism. Figure 13 shows one relevant pushover curve for each of the analyzed bridges.

The corresponding risk indexes in terms of PGA and T_R (RI_{PGA} or RI_{TR}) for both the longitudinal and transversal directions are listed in Table 6.

Table 6. Risk indexes for brittle mechanism.

	Bridge 1		Bridge 2		Bridge 3		Bridge 4		Bridge 5		Bridge 6	
	Long.	Tran.	Long.	Tran.	Long.	Tran.	Long.	Tran.	Long.	Tran.	Long.	Tran.
PGA_C [g]	0.090	0.460	0.043	0.034	0.077	0.077	0.052	0.058	0.094	0.064	0.152	0.573
T_R [years]	14	35,858	43	26	189	189	1063	1746	2316	664	9985	638,303
RI_{PGA} [-]	0.604	3.087	0.289	0.228	0.517	0.517	1.026	1.138	1.302	0.855	2.123	8.031
RI_{TR} [-]	0.178	4.433	0.281	0.229	0.516	0.516	1.048	1.284	1.442	0.864	2.624	14.433

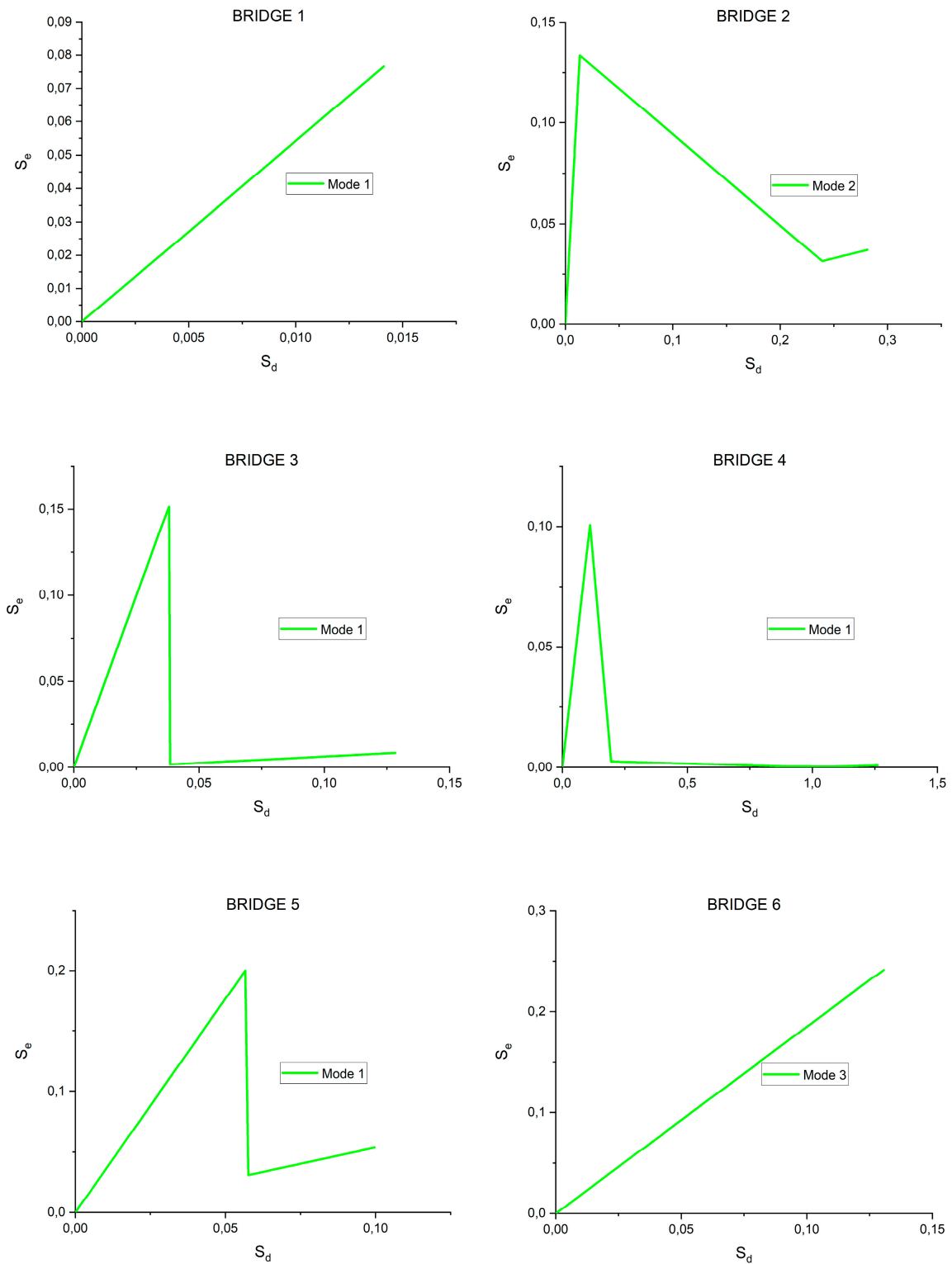


Figure 13. Capacity curves for brittle mechanism (S_e [1/g]– S_d [m]).

5. Discussion

The risk indexes estimated for the six case-studies reflect the well-known seismic deficiencies of existing RC bridges. Looking at the bending (ductile) capacity, all considered viaducts are compliant with the code-prescribed seismic safety level. The piers, properly designed to resist high vertical loads, have a sufficient amount of longitudinal reinforcement to withstand the bending actions generated by the earthquake shaking. Most of the bridges have PGA_C larger than 0.2g. The average value is

0.36 g while the coefficient of variation is 0.39. In general, the higher values of PGA_C refer to short viaducts or characterized by wall-piers. Each analyzed viaduct has a longitudinal and transversal risk index larger than one. On the contrary, shear (brittle) capacity results quite limited. The corresponding PGA_C has average equal to 0.15g and consistently high scatter (1.19 coefficient of variation). In most cases the PGA_C is lower than 0.1g for both longitudinal and transversal directions. Only bridges 4 and 6 present risk indexes larger than one, while the other viaducts are affected by the poor construction details of the piers in terms of transversal reinforcement.

6. Conclusions

In this paper, an efficient procedure to evaluate the seismic vulnerability of existing RC bridges has been described with reference to six typical bridges of the Italian Highway Network. The procedure, based on the modal pushover analysis approach, guarantees a low computational cost resulting in a balanced solution for the assessment of large portfolios of bridges. Risk indexes, expressed in terms of peak ground acceleration or return period, have been calculated (i) considering bending-ductile/shear-brittle collapse mechanisms (ii) for the two principal directions of the structure [32]. The results of the analyses have shown that these bridges are not affected by bending failure of piers (i.e., risk indexes larger than one) but are quite vulnerable with respect to shear-brittle damage. This result reflects the lack of construction details of these types of bridges that were constructed in the post WWII period. These results are not only useful to define the correct seismic retrofitting interventions to be implemented, but are important decision-making parameters for bridge management, investment prioritization and loss assessment at regional scale.

Author Contributions: Conceptualization, P.C. and M.Z.; methodology, M.Z. and N.G.; software, N.G.; validation, P.C.; investigation, all; writing-original draft preparation, N.L., M.Z. and N.G.; writing-review and editing, all; visualization, M.Z. All authors have read and agreed to the published version of the manuscript.

Funding: This research received no external funding.

Conflicts of Interest: The authors declare no conflict of interest.

References

1. Simon, J.; Bracci, J.M.; Gardoni, P. Seismic response and fragility of deteriorated reinforced concrete bridges. *J. Struct. Eng.* **2010**, *136*, 1273–1281. [[CrossRef](#)]
2. De Risi, R.; Di Sarno, L.; Paolacci, F. Probabilistic seismic performance assessment of an existing RC bridge with portal-frame piers designed for gravity loads only. *Eng. Struct.* **2017**, *145*, 348–367. [[CrossRef](#)]
3. Savor Novak, M.; Lazarevic, D.; Atalic, J.; Uros, M. Influence of Multiple-Support Excitation on Seismic Response of Reinforced Concrete Arch Bridges. *Appl. Sci.* **2020**, *10*, 17. [[CrossRef](#)]
4. Berto, L.; Vitaliani, R.; Saetta, A.; Simioni, P. Seismic assessment of existing RC structures affected by degradation phenomena. *Struct. Saf.* **2009**, *31*, 284–297. [[CrossRef](#)]
5. Zucca, M.; Crespi, P.; Longarini, N. Seismic vulnerability assessment of an Italian historical masonry dry dock. *Case Stud. Struct. Eng.* **2017**, *7*, 1–23. [[CrossRef](#)]
6. He, G.L.; Hu, H.H.; Chuang, C.Y.; Huang, C.W. Seismic performance of tall pier bridges retrofitted with lead rubber bearings and rocking foundation. *Eng. Struct.* **2020**, *211*, 110454. [[CrossRef](#)]
7. Wang, Y.; Ibarra, L.; Pantelides, C. Effect of incidence angle on the seismic performance of skewed bridges retrofitted with buckling-restrained braces. *Eng. Struct.* **2020**, *211*, 110411. [[CrossRef](#)]
8. Zucca, M.; Valente, M. On the limitations of decoupled approach for seismic behaviour evaluation of shallow multi-propped underground structures embedded in granular soils. *Eng. Struct.* **2020**, *211*, 110497. [[CrossRef](#)]
9. Zucca, M.; Tropeano, G.; Crespi, P.; Erbi, E. Evaluation of the seismic behavior of multi-propped underground structures embedded in granular soils: A comparison between coupled and decoupled approaches. In Proceedings of the 7th International Conference on Earthquake Geotechnical Engineering, Rome, Italy, 17–20 June 2019.

10. Stochino, F.; Fadda, M.L.; Mistretta, F. Assessment of RC Bridges integrity by means of low-cost investigations. *Frattura ed Integrità Strutturale* **2018**, *46*, 216–225. [[CrossRef](#)]
11. Ministerial Decree (NTC2018). *Updating of Technical Codes for Constructions (in Italian)*; Official Gazette n. 42 of 20/02/18, Ordinary Supplement n. 8; Official Gazette: Rome, Italy, 2018.
12. Kim, S.; D'Amore, E. Push-over Analysis Procedure in Earthquake Engineering. *Earthq. Spectra* **1999**, *15*, 417–434. [[CrossRef](#)]
13. Adhikari, G.; Pinho, R. *Development and Application of Nonlinear Static Procedures for Plan-Asymmetric Buildings*; Research Report No. ROSE-2010/01; ROSE School, IUSS Pavia: Pavia, Italy, 2010.
14. Chopra, A.K.; Goel, R.K. A modal pushover procedure to estimate seismic demands of buildings. *Earthq. Eng. Struct. Dyn.* **2002**, *31*, 561–582. [[CrossRef](#)]
15. Chopra, A.K.; Goel, R.K. A modal pushover analysis procedure to estimate seismic demands for unsymmetric-plan buildings. *Earthq. Eng. Struct. Dyn.* **2004**, *33*, 903–927. [[CrossRef](#)]
16. Paraskeva, T.S.; Kappos, A.J.; Sextos, A.G. Extension of modal pushover analysis to seismic assessment of bridges. *Earthq. Eng. Struct. Dyn.* **2006**, *35*, 1269–1293. [[CrossRef](#)]
17. Paraskeva, T.S.; Kappos, A.J. Further development of a multimodal pushover analysis procedure for seismic assessment of bridges. *Earthq. Eng. Struct. Dyn.* **2009**, *39*, 211–222. [[CrossRef](#)]
18. ATC-40:1996. *Seismic Evaluation and Retrofitting of Concrete Buildings*; 8.1-8.66; Applied Technology Council: Redwood City, CA, USA, 1996.
19. Causevic, M.; Mitrovic, S. Comparison between non-linear dynamic and static seismic analysis of structures according to European and US provisions. *Bull. Earthq. Eng.* **2011**, *9*, 467–489. [[CrossRef](#)]
20. FEMA 356. *Prestandard and Commentary for the Seismic Rehabilitation of Buildings*; Federal Emergency Management Agency: Washington, DC, USA, 2000.
21. FEMA 440. *Improvement of Nonlinear Static Seismic Analysis Procedure*; Applied Technology (ATC-55 Project); Department of Homeland Security, Federal Emergency Management Agency: Washington, DC, USA, 2005.
22. Ministerial Circular (MC2009). *Instruction for the Application of the New Technical Standards for Buildings*; Referred to in the Ministerial Decree of 14 January 2008 (in Italian); Official Gazette n. 47 of 26/02/2009, Ordinary Supplement n. 27. Official Gazette: Rome, Italy, 2009.
23. Verderame, G.M.; Stella, A.; Cosenza, E. Le proprietà meccaniche degli acciai impiegati nelle strutture in cemento armato realizzate negli anni '60. In Proceedings of the X Convegno Nazionale “L’Ingegneria Simica in Italia”, Potenza and Matera, Italy, 9–13 September 2001.
24. Longarini, N.; Crespi, P.; Zucca, M.; Giordano, N.; Silvestro, G. The advantages of fly ash use in concrete structures. *Inz. Miner.* **2014**, *15*, 141–145.
25. Kent, D.C.; Park, R. Flexural members with confined concrete. *J. Struct. Div.* **1971**, *97*, 1969–1990.
26. Park, R.; Paulay, T. *Reinforced Concrete Structures*; John Wiley and Sons: New York, NY, USA, 1973.
27. MIDAS Civil Analysis Reference. 2020.
28. EN 1337-3:2005. *Structural Bearings—Part 3: Elastomeric Bearings*; CEN (European Committee for Standardization), Management Centre: Brussels, Belgium, 2005.
29. EN 1998-2:2005. *Eurocode 8: Design of structures for earthquake resistance—Part 2: Bridges*; CEN (European Committee for Standardization), Management Centre: Brussels, Belgium, 2005.
30. EN 1998-3:2005. *Eurocode 8: Design of Structures for Earthquake Resistance—Part 3: Assessment and Retrofitting of Buildings*; CEN (European Committee for Standardization), Management Centre: Brussels, Belgium, 2005.
31. Italian Civil Protection Ordinanza n. 3274/2003—Articolo 2, commi 3 e 4, D.M.14/1/2008—Scheda di sintesi della verifica sismica di “livello 1” o di “livello 2” per i ponti strategici ai fini della protezione civile o rilevanti in caso di collasso a seguito di evento sismico (In Italian), 2008.
32. Valente, M.; Milani, G. Alternative retrofitting strategies to prevent the failure of an under-designed RC frame. *Eng. Fail. Anal.* **2018**, *89*, 271–285. [[CrossRef](#)]

